scientific reports

Check for updates

OPEN

Optimization for next generation laptops enhancing performance and compactness

Devisowjanya P[1]✉, Aishwarya N[1], Bhanu Sai Mani Kiran B[1], Lokesh Kumar K.M[2] & Arun AAdhithyan S.J[1]

This paper presents a computational intelligence-optimized multiband MIMO antenna for next-generation laptops, addressing the demand for compact, high-performance, and multiband wireless connectivity. The proposed 4-port MIMO configuration, with an overall footprint of $94.1 \times 28.29 \times 0.8$ mm³, is optimized for seamless integration along the laptop's top edge, where minimal width is crucial. It supports operation at 2.45 GHz, 5 GHz, and 6 GHz, enabling compatibility with dual and tri-band Wi-Fi 6E routers. To accelerate the design process and reduce manual iteration, machine learning (ML) algorithms including AdaBoost, SVM, CatBoost, and Decision Trees were employed. A simulation dataset was generated in CST studio by systematically varying critical antenna parameters. This dataset was used to train the ML models, enabling them to learn the nonlinear relationships between geometry and performance metrics such as S-parameters, gain, efficiency, envelope correlation coefficient (ECC), diversity gain. Upon training, the models predicted optimal design parameters for desired performance goals. The resulting antenna exhibited isolation greater than 16 dB, ECC below 0.08, and a measured realized gains of 0.73, 2.1, and 3 dBi across the operating bands. In addition, the channel capacity loss remained under 0.35 bits/s/Hz, confirming strong MIMO performance. This work highlights that incorporating computational intelligence into antenna design not only expedites the development process but also improves system efficiency, providing a scalable and intelligent solution for next-generation multifunctional, high-speed laptop platforms.

In today's hyper-connected digital era, antennas are essential for maintaining continuous communication for portable devices like laptops. To enable wireless access to the internet through local area networks (LAN), laptops require efficient antennas capable of supporting multiple frequencies, ensuring stable connections and high data speeds. For data-intensive tasks such as online gaming, streaming, and video conferencing, multiple input multiple output (MIMO) technology must be integrated into laptops utilizing multiple antennas. Additionally, to support evolving applications like virtual reality (VR), augmented reality (AR) as well as wireless content streaming from laptops to external devices such as projectors or TVs, low-latency antennas are essential. Hence, compact, multiband MIMO antennas with low latency, and high diversity gain are essential to effectively address these challenges[1].

The state-of-the-art research discusses MIMO antennas with spatial diversity, as reported in[1–5]. A compact, sub-6-GHz MIMO four-element antenna that can operate at dual frequencies for 5G laptops as reported in[1] meets high screen-to-body ratio requirements, making it suitable for narrow-bezel laptop designs. The study presented in[2] explores key MIMO and spatial diversity technologies in antenna design, analyzing how spatial diversity enhances MIMO performance and supports efficient information transmission in networks. A low profile, quad-element MIMO for 5G laptops, achieving over 10 dB isolation within 3300–3600 MHz and 4800–5000 MHz, with a height of 1.4 mm for compatibility with large display-to-body ratio designs, is presented in[3]. An ultra-wideband (UWB), dual-element MIMO antenna, utilizing metamaterials to enhance inter-antenna coupling, was reported in[4]. A review paper presented in[5] discusses MIMO antenna designs, highlighting UWB, dual-band, and circularly polarized antennas along with their isolation, gain, efficiency, and potential applications for 5G, 6G, and various wireless technologies. However, these papers primarily focus on antennas for Wi-Fi4, with no consideration for upgrading capabilities.

[1]Department of ECE, Amrita School of Engineering, Amrita Vishwa Vidyapeetham, Chennai, India. [2]School of Computer Science, University of Guelph, Guelph, Canada. ✉email: p_devisowjanya@ch.amrita.edu

The introduction of Wi-Fi as an alternative to Ethernet cables significantly improved connectivity and data speeds in laptops. Early Wi-Fi 4 operated at 2.45 GHz and offered speeds of up to 600 Mbps. As data congestion increased, Wi-Fi operating at 5 GHz, offering 3.5 Gbps, was introduced. To further enhance speeds to 9.6 Gbps, Wi-Fi 6 and 6E were developed, operating at a carrier frequency of 6 GHz[6]. To handle the growing volume of data, the Wi-Fi family continues to evolve. Consequently, laptop antennas must also be regularly updated to support these advancements. Multiband antennas[7–11], capable of harnessing signals from dual-band and tri-band routers, are preferred. Integrating multiband functionality (operating at Wi-Fi 6 and 6E) with MIMO antennas[12–17] enhances both throughput and transmission rate. However, designing multiband MIMO antennas involves trade-offs between size, bandwidth, isolation, and gain, often resulting in time-consuming and inefficient design processes. To address these challenges, computational intelligence techniques can be employed to optimize critical parameters such as size, performance metrics, and radiation patterns, significantly reducing design time while enhancing overall antenna performance[18].

Machine learning (ML) algorithms have emerged as powerful tools to overcome the complexities and time-consuming nature of traditional design processes. By leveraging various ML approaches, key antenna parameters, including size, bandwidth, isolation, gain, envelope correlation coefficient (ECC) and diversity gain (DG) can be optimized to meet the multifunctional demands of modern laptops. The state-of-the-art research explores different ML techniques[19–26] and their impact on design efficiency and antenna performance. A ML-assisted optimization method (MLAO) was reported in[19], predicting and optimizing the responses of antennas and their arrays using multilayer approaches. In[20], MLAO was integrated with convolutional neural networks (CNNs) and Gaussian process regression (GPR) to develop a surrogate model for analyzing multiband and broadband antenna designs. The ML algorithm used in[21] transformed the design process of slotted waveguide antennas (SWAs) into a regression problem, predicting slot lengths and displacements based on sidelobe level ratios and resonant frequencies. This approach accelerated the design process and achieved high accuracy and efficiency. Advanced ML algorithms, particularly deep neural networks, were used in[22] to determine the effectiveness of AI-driven methodologies in addressing user-induced challenges in antenna design evolution from GSM to 5G technologies. The work in[23] employed modern ML techniques, including lasso regression, artificial neural networks (ANNs), and k-nearest neighbor (kNN) methods, to optimize design parameters for a double T-shaped antenna that operates at two frequencies. A UWB MIMO antenna[24] is optimized through different ML algorithms such as artificial neural network (ANN), extreme gradient boosting (XGBoost), random forest (RF), K-nearest neighbor (KNN), and Decision Tree (DT) to predict only the S parameters. The geometry of a patch antenna[25] operating at WiMAX/WLAN was optimized using Polynomial Regression, Decision Tree, Random Forest, XGBoost ML models. The optimized parameters of XGBoost are in close agreement in both train and test cases. A review paper on ML-assisted and conventional approaches for 5G antenna types, highlighting the role of ML in categorizing, analyzing, and enhancing modern antenna configurations was presented in[26]. However, the state-of-the-art research has not addressed multiband MIMO antennas, highlighting a gap in the literature regarding their design, optimization, and performance evaluation using computational intelligence techniques.

In this paper, the proposed MIMO antenna is well-suited for modern laptop applications due to its compact design, multi-band operation, and high isolation. It operates at 2.45 GHz, 5 GHz, and 6 GHz, supporting legacy and emerging wireless standards such as Wi-Fi (including Wi-Fi 6/6E) and Bluetooth, making it ideal for continuous wireless connectivity in portable devices. Its small footprint ensures compatibility with space-constrained laptop interiors, while the optimized element spacing enhances spatial diversity, resulting in improved data throughput and reliability in multi-path rich indoor environments. The use of machine learning for parameter optimization allows the design to adapt efficiently to new frequency requirements, enabling future-proof integration into next-generation laptop platforms. The subsequent section of the paper is organised as follows: in "Antenna design" section covers single antenna and MIMO antenna designs. In "Machine learning-assisted optimization" section details the ML techniques used for predicting antenna parameters. In "Testing and measurement" section presents the fabrication results of the computational intelligence-optimized multiband (CIOM) MIMO antenna, based on the ML-predicted outcomes.

Antenna design

The proposed MIMO antenna targets Wi-Fi 6E laptop application focusing on multi-band capability. It is specifically designed with compact dimensions to fit within the limited space available on the laptop's top edge panel without interfering with other components. Its low-profile form factor (0.8 mm thickness) facilitates easy integration behind the display bezel. As for thermal concerns, the antenna structure is implemented on an FR4 substrate with no active components, thus minimizing self-heating. In practical deployments, the antenna is positioned away from heat-generating components like the CPU/GPU to avoid thermal interference. Furthermore, the use of machine learning for parameter optimization allows the design to adapt efficiently to new frequency requirements, enabling future-proof integration into next-generation laptop platforms.

Multiband antenna

To meet the requirements of modern laptops for a compact, multi-band, and omnidirectional antenna with an average gain comparable to an isotropic radiator, a monopole antenna with interconnected stubs is proposed, as shown in Fig. 1. This antenna is designed to operate at 2.45, 5, and 6 GHz, achieving gains greater than 1 dBi across all bands to reliably capture signals from dual-band and tri-band routers. With compact dimensions of 22×28 mm^2 and fabricated on an FR4 substrate with a thickness of 0.8 mm, the antenna ensures a low-profile footprint suitable for integration within laptops. The multi-band response is achieved by incorporating a rectangular stub, a meandered C-shaped stub, and a rectangular slot within the radiating patch. Specifically, the rectangular patch influences the 5 GHz band, the meandered C-shaped stub is tuned for the 6 GHz band, and the side rectangular slots primarily affect the 2.45 GHz band. By adjusting the dimensions of these structures,
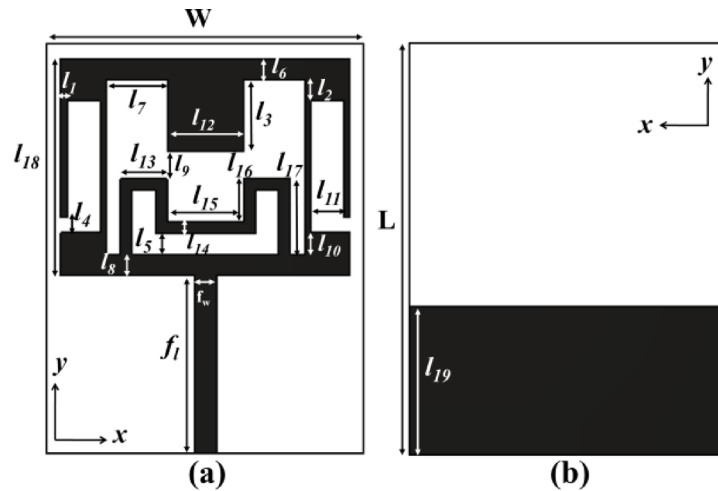
Fig. 1. Multi-band antenna (**a**) front view (**b**) rear view (black is copper, white is FR4).
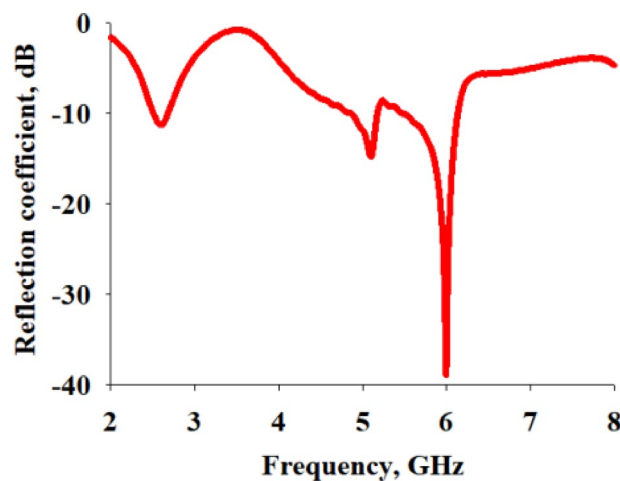

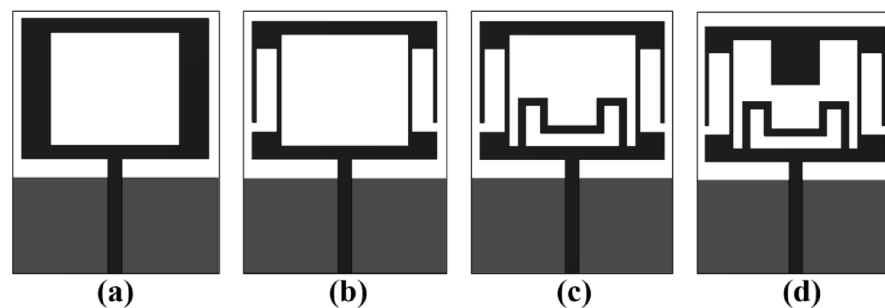**Fig. 2**. Simulated reflection coefficients of single antenna.

Fig. 3. Evolution of the antenna. (**a**) Antenna 1 (**b**) Antenna 2 (**c**) Antenna 3 (**d**) Proposed antenna.

the antenna exhibits the desired tri-band performance. The simulated reflection coefficients of the single element antenna are shown in Fig. 2.

Evolution of multiband antenna

The step-by-step evolution of the proposed antenna is illustrated in Fig. 3 to clearly demonstrate the role of the rectangular stub, meandered stub, and rectangular slots in achieving the desired multiband performance. Initially, a monopole concentric rectangular patch, as shown in Fig. 3a, is designed to operate close to 2.45 GHz,
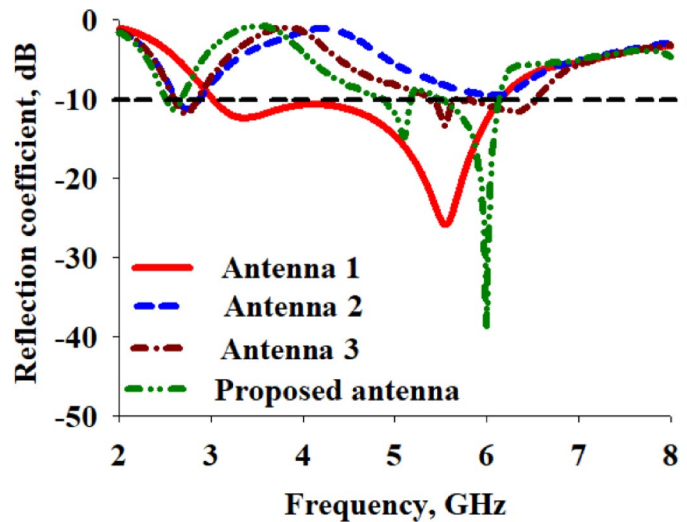
3

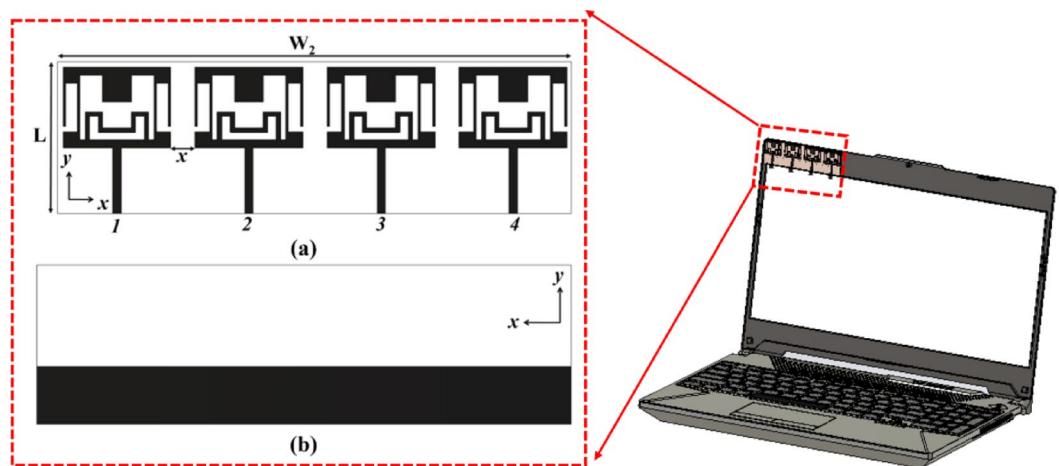**Fig. 4**. Reflection coefficients of the evolution of the multiband antenna.

Fig. 5. 4 element MIMO antenna (**a**) front view (**b**) rear view (black is copper, white is FR4).

5 GHz, and 6 GHz. Owing to the inherent wideband characteristics of the monopole structure, the antenna exhibits a broad operating frequency range extending from 3 to 6 GHz, thereby offering a bandwidth of nearly 3 GHz. However, to enhance the frequency selectivity and achieve distinct multiband operation rather than a wideband response, further structural modifications are introduced in subsequent stages. In the next stage, as shown in Fig. 3b, a rectangular slot is inserted into the side arms of the patch. This modification significantly alters the current distribution on the radiator and successfully introduces a new resonance around 2.5 GHz. To further improve the antenna performance at higher frequencies, a meandered stub is incorporated at the bottom of the patch, as illustrated in Fig. 3c. This addition enables the antenna to resonate effectively at 6 GHz, contributing to the desired multiband behavior. Finally, to generate an additional resonance in the mid-frequency range, a rectangular stub is positioned on the top of the patch, as depicted in Fig. 3d. This structural inclusion results in a clear resonance at 5 GHz. The effectiveness of each evolutionary step and the improvement in multiband characteristics are validated through the corresponding reflection coefficients, which are presented in Fig. 4.

MIMO antenna

To enable spatial diversity and enhance data throughput in laptop applications, a MIMO configuration is developed by placing four of these multi-band elements at an optimized spacing x. The overall MIMO antenna dimensions are set to 94.18×28 mm^2, allowing seamless integration along the laptop's top edge where width is a critical constraint as illustrated in Fig. 5. Instead of relying on additional decoupling structures, inter-element isolation is managed by fine-tuning the spacing between elements. This spatial arrangement helps minimize mutual coupling and latency while improving isolation and diversity characteristics. The novelty of the proposed work lies in the integration of computational intelligence (ML) with multiband MIMO antenna design, enabling automatic prediction of optimal design parameters to meet multiple performance metrics (S_{11}, ECC, DG,

efficiency, and isolation) simultaneously. Unlike existing works that primarily rely on iterative manual tuning or single-band optimization, this work systematically reduces design iterations and enhances reliability by leveraging ML-driven predictions validated through fabrication.

Dataset generation

To generate the dataset using Computer Simulation Technology (CST) Microwave Studio 2023, an existing multi band antenna was identified in Antenna Magus as shown in Fig. 1. The design comprised a rectangular stub, a meandered C-shaped stub, and a rectangular slot each contributing to the antenna's resonance behavior at three target frequencies. Key geometric parameters affecting these features were identified and defined as h_1–h_4, h_6, h_8, s_1–s_3, w_1–w_3. These parameters were organized by grouping (l_1 to l_{19} and f_1), as shown in Table 1, into clusters. These parameters were carefully chosen to represent key dimensional variations across all major substructures of the antenna, including the two stubs and slot. These parameters, though not grouped by substructure, collectively influence the antenna's performance by altering effective current paths, coupling, and resonance characteristics. Modifying these parameters impacts performance metrics such as return loss (S_{11}), voltage standing wave ratio (VSWR), gain, isolation (S_{12}), efficiency, ECC, and DG in the required operating frequencies. To assess MIMO performance, an additional parameter x was introduced to vary the inter-element spacing between antenna elements. This spacing directly influences mutual coupling, ECC, and overall diversity behavior in MIMO scenarios. Each parameter was assigned a practical range based on fabrication feasibility and RF performance. Parametric sweeps were then performed, simulating the antenna for each combination to generate a comprehensive dataset for machine learning model training and performance analysis. Each simulation in CST was carried out using frequency-domain solvers. For each variation, far-field data and S-parameters were extracted directly within CST. The ECC and diversity gain were computed using CST's built-in post-processing templates, which utilize far-field radiation data for the selected ports. The extracted results for all parameter combinations were compiled to form a comprehensive dataset.

The dataset was then used to train machine learning algorithms, which learned the mapping between geometric parameters and key performance metrics such as S_{11}, S_{12}, ECC, VSWR, efficiency, gain, and diversity gain. The trained machine learning models enabled the identification of optimal design parameter combinations that meet specific performance goals, namely: $S_{11} < -12$ dB, ECC < 0.5, DG > 9 dB, efficiency $> 80\%$, and isolation > 15 dB at the 2.45 GHz, 5 GHz, and 6 GHz operating bands. These model-predicted parameters were then validated through full-wave simulations in CST Studio Suite. Upon confirming that the simulated results satisfied the target specifications, the antenna was fabricated for experimental validation. This data-driven approach is particularly beneficial for designing compact MIMO antennas intended for integration into laptops, where constraints on space and performance are stringent. Moreover, it offers flexibility to adapt to evolving wireless standards such as the introduction of Wi-Fi 6E, which operates in the 6 GHz band by allowing the antenna to be re-optimized to accommodate additional frequency bands beyond the traditional 2.4 GHz and 5 GHz Wi-Fi bands.

Machine learning-assisted optimization

In this section, various regression algorithms are applied to a custom-created dataset to determine the antenna dimensions. The optimized dimensions predicted by the best-performing model are then used for RF antenna simulation and fabrication. In order to achieve this, various machine learning algorithms like decision tree, SVM, linear regression and gradient boosting techniques (XGBoost and CatBoost) are employed[27]. Linear regression (LR) is a supervised ML algorithm that fits a linear equation to relate input and target variables. A SVM utilizes either a linear or non-linear kernel to establish this relationship, while Decision Trees (DT) use a binary tree structure to map inputs to outputs. Gradient boosting algorithms, such as XGBoost (XGB) and CatBoost (CB), iteratively improve predictions by minimizing errors in successive models.

In the context of MIMO antenna design, these ML algorithms are used to model the relationship between antenna operational parameters (independent features) and antenna design parameters (dependent target variables). Independent features include functional parameters of antennas, such as reflection coefficients (s_{ii}), transmission coefficients (s_{ij}), VSWR, realized gain, efficiency, ECC and DG while target variables represent grouped antenna dimensions that, when designed and simulated, achieve the desired performance outcomes. To ensure precise predictions, regression models are built for each grouped target parameter.

Figure 6 depicts the end-to-end machine learning workflow for antenna parameter optimization. It starts with the collection of data for CST simulation, in which important antenna performance parameters such as h_1–h_8, s_1–s_3, w_1–w_3, x is extracted. Then, the data are pre-processed into features for input and target dimensions. Multiple regression models are then trained and tested using default hyperparameters. The model's predictions

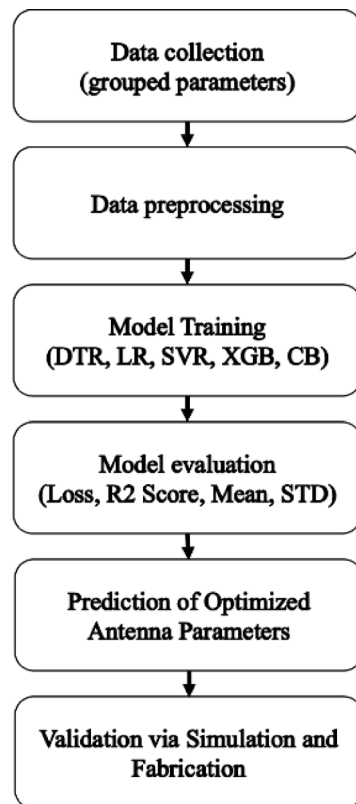| h_1	h_2	h_3	h_4	h_6	h_8	s_1	s_2	s_3	w_1	w_2	w_3	x
l_6	l_1	l_7	l_5	l_5	l_3	l_1	l_2	l_4	l_7	l_{18}	l_{18}	x
l_8	l_{11}	l_9	l_9	l_{16}	l_9	l_{11}	l_{10}		l_{12}	f_1	l_{19}	
l_9	l_{12}	l_{12}	l_{17}						l_{13}		f_1	
	l_{15}	l_{13}							l_{15}			
		l_{14}										
		l_{15}										

Table 1. Grouped parameters.

Fig. 6. End-to-end machine learning workflow for antenna parameter optimization.

result is then employed to predict the optimized antenna dimensions, which are first validated through CST simulation and afterward by actual fabrication. Such a systematic pipeline assures the accuracy, generalizability, and practical fabricability of the proposed ML-driven antenna design.

All the regression algorithms were trained on default hyper parameters (listed in Table 2) to ensure the validity of the experiment. Tables 3 and 4 provide the performance comparative analysis of the models in terms of mean square error (MSE) and R² score for predicting the antenna dimensions. Best performing values are highlighted in bold. MSE[28] defined in Eq. (1) measures the average squared difference between the predicted and actual grouped antenna dimensions. Mathematically, it is given as,

$$MSE = \frac{1}{n} \sum_{j=1}^{n} \left(AD_j - \widehat{AD_j} \right)^2 \tag{1}$$

where AD_j represents the actual dimension value for the jth sample, $\widehat{AD_j}$ denotes the predicted value and *n* is the total number of samples used in the experiment. Another measure to evaluate the quality of regression model is R² score. This metric in Eq. (2) explains the proportion of variance in the actual antenna dimensions and assesses how well the model generalizes. A value closer to 1 indicates better predictions, while a value of 0 implies that the model captures none of the variance. R² score is given as,

$$R^2_{\text{score}} = 1 - \frac{\sum_{j=1}^{n} \left(AD_j - \widehat{AD_j} \right)^2}{\sum_{j=1}^{n} \left(AD_j - \overline{AD_j} \right)^2} \tag{2}$$

Table 5 presents the mean and standard deviation (STD) of predictions for grouped antenna design parameters across five different regression algorithms such as decision tree regressor (DTR), linear regression (LR), support vector regressor (SVR), XGBoost (XGB) and CatBoost (CB). The mean column shows the average predicted values across 5 validation folds and the STD column reflects the variation in the predictions, thereby indicating model stability and generalization ability. It is evident from Table 5 that CB achieves high mean prediction accuracy and low standard deviation across most parameters, highlighting its robustness. XGB follows closely, also demonstrating strong performance. Thus, the ML model which has lowest error, high R² score and consistent performance across cross-validation folds is identified as the robust and reliable model for optimizing MIMO antenna design parameters.

Model name	Hyperparameters	Default values
Linear regression	copy_x	TRUE
	fit_intercept	TRUE
	n_jobs	None
	positive	FALSE
Support vector machine	C	1
	Gamma	Scale
	kernel	RBF
Decision tree	criterion	Squared error
	splitter	Best
	max depth	None
	min sample split	2
XGBoost	booster	gbtree
	eta	0.3
	gamma	0
	max_depth	6
	objective	Squared error
	eval_metric	RMSE
CatBoost	iterations	Dynamic
	learning_rate	Dynamic
	loss_function	RMSE
	depth	Dynamic

Table 2. Grouped parameters.

S. no.	AD	LR	SVM	DT	CB	XGR
1	h_1	0.0261	0.0113	0.0038	**0.0022**	0.0023
2	h_2	0.3357	0.072	0.0253	**0.0152**	0.0162
3	h_3	0.2129	0.0811	0.0439	**0.0273**	0.0274
4	h_4	0.0646	0.034	0.0248	**0.0181**	0.0183
5	h_6	0.0653	0.0465	0.0437	**0.0322**	0.0328
6	h_8	2.4103	1.544	0.4349	0.3755	**0.3183**
7	s_1	0.2537	0.1742	0.0626	0.0362	**0.0311**
8	s_2	0.7651	0.183	0.0159	**0.0139**	0.0154
9	s_3	2.654	0.5212	0.079	**0.0329**	0.043
10	w_1	0.0833	0.0624	0.0507	0.0364	**0.0338**
11	w_2	0.0985	0.0981	0.108	**0.1081**	0.1095
12	w_3	0.0985	0.0982	0.2041	**0.1096**	0.1147
13	x	25.6811	6.803	0.349	**0.2821**	0.3747

Table 3. Comparative analysis of all the models in terms of loss.

Testing and measurement

The optimized MIMO antenna parameters predicted by the ML algorithm, are entered into the CST simulation software. Further optimizations are carried out around the ML-predicted values to align with the target application requirements. The optimized dimensions of the CIOM MIMO antenna are shown in Table 6. The impedance matching, radiation pattern, and MIMO parameters are analyzed to ensure they meet the desired specifications for laptop applications. The simulated results indicate good impedance matching across the three proposed bands, an isolation more than 16 dB, realized gain over 0.73 dBi, ECC lesser than 0.01, and a DG above 9.8 dB. Figure 7 shows the fabricated CIOM MIMO antenna which was subsequently tested as a prototype. The measured results of the fabricated prototype were compared against the simulation results to study the real-world performance of the MIMO antenna.

Impedance matching and isolation

The impedance matching and isolation characteristics of the proposed CIOM MIMO antenna (in Fig. 8c) were evaluated through simulations using CST 2023 and measurements conducted with a Keysight PNA Vector Network Analyzer (N5227B). The reflection coefficients (s_{ii}), as shown in Fig. 8a, demonstrate good impedance matching across the desired frequency bands, with values below − 10 dB. This indicates efficient power transfer

S. no.	AD	LR	SVM	DT	CB	XGR
1	h_1	0.0927	0.6061	0.8704	**0.9294**	0.9214
2	h_2	0.1034	0.8077	0.9323	**0.9738**	0.9568
3	h_3	0.0055	0.6211	0.7954	**0.9142**	0.8905
4	h_4	0.016	0.4822	0.6263	**0.7769**	0.7213
5	h_6	0.0049	0.2912	0.3458	**0.6312**	0.5156
6	h_8	0.0292	0.3782	0.8194	**0.9211**	0.8718
7	s_1	0.0636	0.3572	0.7687	**0.8879**	0.8851
8	s_2	0.0892	0.7822	0.981	**0.9927**	0.9817
9	s_3	0.0893	0.8211	0.9734	**0.992**	0.9853
10	w_1	0.0016	0.2515	0.4158	**0.7037**	0.5944
11	w_2	− 0.0036	**− 0.0003**	− 0.0998	**− 0.0622**	− 0.1156
12	w_3	− 0.0036	**− 0.0003**	− 1.0679	**− 0.5749**	− 0.1693
13	x	0.2979	0.814	0.9902	**0.9969**	0.9898

Table 4. Comparative Analysis of all the models in terms of R^2 score.

Model target	Mean					STD				
	DTR	LR	SVR	XGB	CB	DTR	LR	SVR	XGB	CB
h1	0.8712	0.0660	0.6104	0.9274	0.9513	0.0118	0.0113	0.0041	0.0102	0.0037
h2	0.9370	0.1135	0.8119	0.9567	0.9722	0.0053	0.0115	0.0072	0.0019	0.0019
h3	0.8036	0.1040	0.6257	0.8588	0.9162	0.0181	0.0041	0.0179	0.0043	0.0201
h4	0.6021	0.0060	0.5016	0.7316	0.7323	0.0247	0.0053	0.0100	0.0229	0.0188
h6	0.4302	0.0026	0.3064	0.5506	0.5558	0.0442	0.0041	0.0037	0.0194	0.0320
h8	0.8367	0.0248	0.3816	0.8850	0.9266	0.0199	0.0047	0.0181	0.0053	0.0068
s1	0.7868	0.0538	0.3753	0.8894	0.9113	0.0115	0.0106	0.0197	0.0065	0.0077
s2	0.9768	0.0845	0.7814	0.9829	0.9906	0.0018	0.0057	0.0064	0.0024	0.0054
s3	0.9757	0.0925	0.8191	0.9856	0.9926	0.0027	0.0089	0.0045	0.0011	0.0009
w1	0.4031	0.0047	0.2749	0.6015	0.7033	0.0082	0.0031	0.0230	0.0101	0.0169
w2	− 0.0422	− 0.0041	− 0.0008	− 0.2011	− 0.2011	0.0326	0.0009	0.0008	0.0083	0.0093
w3	− 1.1428	− 0.0040	− 0.0009	− 0.1608	− 0.2859	0.0246	0.0006	0.0005	0.0110	0.0127
x	0.9840	0.2919	0.8121	0.9903	0.9962	0.0024	0.0108	0.0076	0.0005	0.0003

Table 5. Mean and standard deviation (STD) of predicted grouped antenna parameters across fivefold cross-validation.

Parameter	Dim. (mm)	Parameter	Dim. (mm)	Parameter	Dim. (mm)
l_1	0.43	l_{10}	1.5	l_{19}	11
l_2	1.5	l_{11}	2.27	f_1	12.29
l_3	5	l_{12}	5.32	f_w	1.5
l_4	1	l_{13}	3.21	W	22
l_5	1.39	l_{14}	0.81	L	28.29
l_6	1.48	l_{15}	5.32	x	4.06
l_7	4.21	l_{16}	3	W_2	94.1
l_8	1.43	l_{17}	5.19		
l_9	1.85	l_{18}	15		

Table 6. Optimized antenna dimensions. *Dim.* Dimensions.

at the operating frequencies of 2.45 GHz, 5 GHz, and 6 GHz. The bandwidth over which this impedance matching is maintained is sufficient for the intended laptop application. The measured transmission coefficients, as depicted in Fig. 8b, is less than − 16 dB, indicating maximum isolation among the elements. This high isolation results in a low ECC and enhances the overall MIMO performance by improving diversity gain. A comparison of the simulated and measured results confirms that the antenna meets the design specifications and operates effectively across the targeted frequency bands, thereby fulfilling the performance requirements for laptop-based 5G applications.
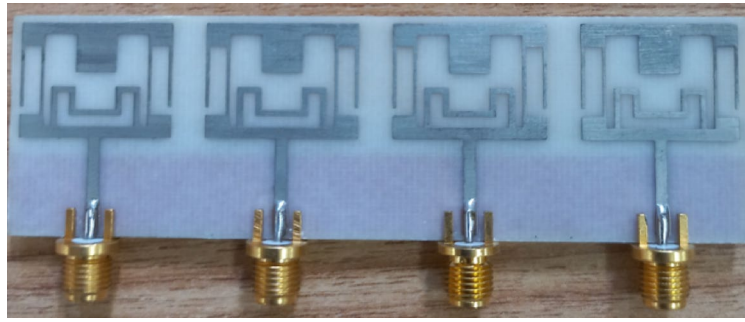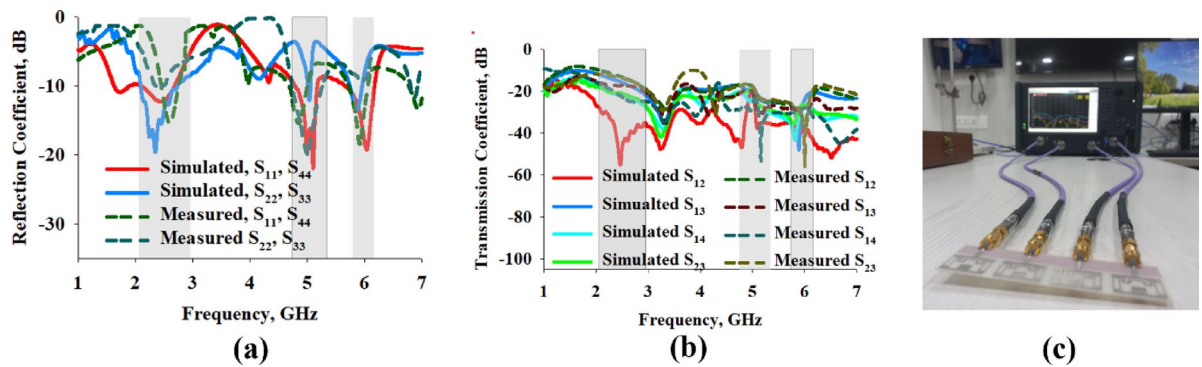
Fig. 7. Fabricated MIMO antenna.

Fig. 8. Simulated and measured (**a**) reflection coefficients (**b**) transmission coefficients of the MIMO antenna. (**c**) Antenna under measurement.

Radiation pattern

The prototype CIOM MIMO antenna was evaluated in an anechoic chamber to analyse its radiation characteristics. The antenna exhibits an omnidirectional radiation pattern, radiating uniformly in the azimuthal direction (horizontal, H-plane) and forms an elongated eight-shaped pattern in the elevation direction (vertical, E-plane). This characteristic is highly desirable for laptops, as it ensures signal reception from multiple directions. The radiation patterns for Port 1 at 2.45, 5, and 6 GHz are presented in Fig. 9 as polar plots for both simulated and measured values. Discrepancies between them are attributed to fabrication tolerances and constraints in the measurement setup. Additionally, Fig. 10 depicts the measured and simulated realized gain on left y axis. The right y axis depicts the simulated radiation efficiency. The results show that the measured realized gain and the radiation efficiency exceed 0.73 dBi and 78%, respectively, across all target frequencies. This ensures minimal power loss and consistent radiation in the horizontal plane while maintaining omnidirectional coverage. Notably, the CIOM MIMO antenna attains a maximum gain of 3 dBi at 6 GHz, further validating its suitability for laptop applications.

ECC and DG

Maintaining proper isolation between antennas in a MIMO system is crucial for achieving optimal performance, as poor isolation can lead to significant interference and degrade system functionality. Isolation is typically evaluated using two important parameters: the ECC and DG. The level of correlation between signals transmitted or received by different antenna elements is quantified by ECC. For efficient MIMO operation, an ECC value less than 0.5 is highly desirable, as it indicates minimal interference and ensures the independence of the antenna elements. This low ECC helps to improve the overall signal quality and enhances data transmission. Similarly, DG measures the improvement in signal robustness and reliability achieved through the use of multiple antennas. High DG values reflect the antenna system's ability to mitigate fading and interference effectively. Together, low ECC and high DG significantly enhance the performance of MIMO systems, ensuring better connectivity and reliability. The ECC and DG[29] is evaluated using far-fields, as the efficiency of the CIOM MIMO antenna remains below 90% across two frequencies, with the corresponding equations provided in Eqs. (3) and (4).

$$\rho_e = \frac{\left| \iint \left[\overrightarrow{F_1}(\theta, \phi) \cdot \overrightarrow{F_2}(\theta, \phi) \right] d\Omega \right|^2}{\iint \left| \overrightarrow{F_1}(\theta, \phi) \right|^2 d\Omega \iint \left| \overrightarrow{F_2}(\theta, \phi) \right|^2 d\Omega} \tag{3}$$

Fig. 9. Simulated and measured radiation pattern at port 1 (**a**) 2.45 GHz (**b**) 5 GHz (**c**) 6 GHz. (**d**) Antenna measurement in anechoic chamber.
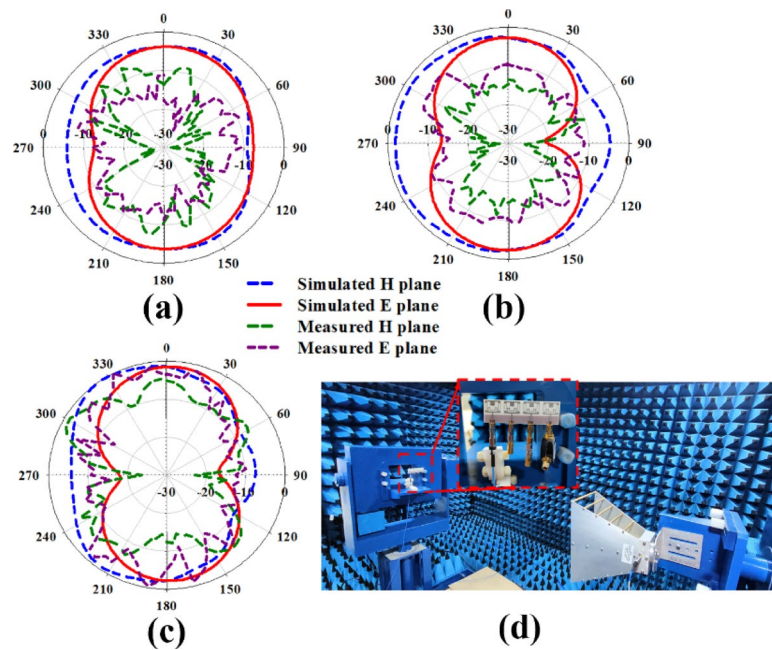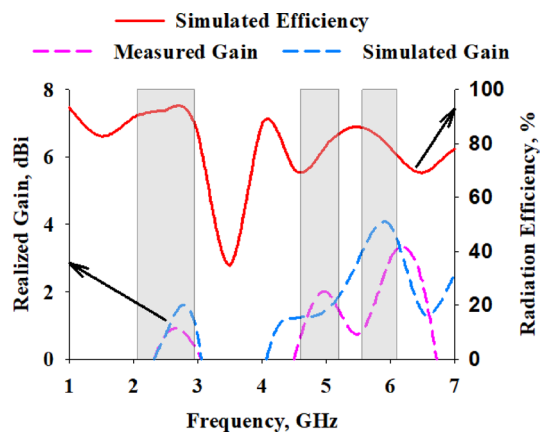

Fig. 10. Simulated and measured radiation pattern at port 1 (**a**) 2.45 GHz (**b**) 5 GHz (**c**) 6 GHz. (**d**) Antenna measurement in anechoic chamber.

$$DG = 10\sqrt{1 - |\rho_e|^2} \qquad (4)$$

The ECC and DG values of the CIOM antenna are illustrated in Fig. 11. These values are calculated using the inbuilt post-processing template within CST. The ECC between antenna elements 1 and 2 is observed to be less than 0.08 at 2.45, 5, and 6 GHz, ensuring minimal signal interference and high isolation between the antennas. Additionally, the DG is consistently greater than 9.4 across these frequencies, which highlights the system's ability to effectively combat multipath fading and maintain robust signal quality. These results shown in Table 7 confirm the proposed MIMO antenna's suitability for applications requiring high performance, such as laptops operating in multi-band wireless communication systems.

The proposed work is compared with the existing State of the Art and presented in Table 8. The proposed work provides better isolation and ECC compared to most of the papers[1,3,13,14,16,17] without adding any decoupling structures. The width of the MIMO antenna[13–17] in the literature is less compared to the proposed work as they have placed around the display screen, while the proposed work is placed on the edge of the panel to avoid any interferences with other components.
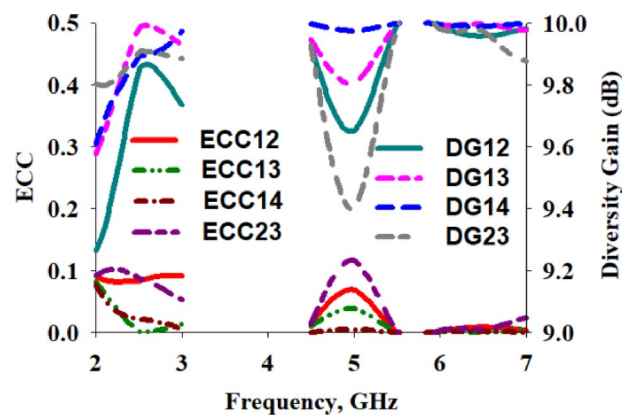
Fig. 11. Simulated ECC and DG of the CIOM MIMO antenna.

Frequency (GHz)	Isolation (dB)	ECC	DG (dB)	Gain (dBi)	Simulated radiation efficiency (%)
2.45	> 16	0.08	9.4	0.73	92
5	> 20	0.06	9.8	2.1	80
6	> 22	0.01	9.9	3	78

Table 7. Summarization of MIMO parameters.

Refs.	Single element dimensions (mm × mm)	Frequency (GHz)	Isolation (dB)	Gain (dBi)	ECC	DG (dB)	ML-driven predictions
[1]	0.17λ × 0.03λ	3.4–3.8, 4.8–5	> 10	–	< 0.27	–	No
[3]	0.33λ × 0.03λ	3.3–3.6, 4.8–5	> 10	–	< 0.3	–	No
[13]	0.17λ × 0.03λ	0.85–1, 1.45–2.83, 4.4–7.4	> 14	> 2.3	< 0.5	–	No
[14]	0.24λ × 0.08λ	2.4, 5, 6	> 11	2.41	< 0.3	–	No
[15]	0.18λ × 0.04λ	0.88–0.96, 1.7–2.6, 4.4–5, 6.2–7.1	> 17	> 2.5	< 0.4	–	No
[16]	0.18λ × 0.04λ	0.74–0.99, 1.38–2.64, 4.3–4.7, 4.8–6.5	> 10	> 2.59	< 0.5	–	No
[17]	0.14λ × 0.02λ	0.7–1, 1.5–2.5, 4.6–6.5, 7–7.2	> 11	> 1.76	< 0.3	–	No
CIOM	0.18λ × 0.23λ	2.45, 5, 6	> 16	> 0.73	< 0.08	> 9.4	Yes

Table 8. Comparison of the proposed work with the state-of-the-art methods.

CCL, MEG and TARC

In addition to conventional metrics such as S-parameters, ECC, and DG, advanced MIMO performance indicators including channel capacity loss (CCL), total active reflection coefficient (TARC), and mean effective gain (MEG) were evaluated[30] to ensure comprehensive performance validation. CCL quantifies the loss in system capacity due to correlation and mutual coupling among antenna elements. For the proposed 4-port MIMO antenna, both simulated and measured CCL values remained below 0.35 bits/s/Hz across all the operating bands (2.45 GHz, 5 GHz, and 6 GHz), as shown in Fig. 12, indicating minimal degradation in channel capacity and ensuring efficient data throughput. TARC, illustrated in Fig. 13, assesses the effective reflection when multiple ports are simultaneously excited, which is critical for multiport systems. The TARC for the proposed antenna was consistently below − 10 dB across the operating frequency range, demonstrating good impedance matching and reduced reflection under active MIMO operation. Additionally, MEG, as depicted in Fig. 14, measures the average gain performance of each antenna element in realistic multipath environments. The MEG values were maintained below − 6 dB, which is within acceptable limits and indicates stable and balanced reception across all antenna ports. These findings affirm the suitability of the proposed antenna design for compact, high-performance laptop applications.

Conclusion

The proposed CIOM MIMO antenna is designed for sub-6 GHz 5G applications, offering compact size, multi-band capability, and suitability for integration into laptop devices. It operates at 2.45 GHz, 5 GHz and 6 GHz with at least 200 MHz bandwidth per band, achieving a minimum realized gain of 0.73 dBi and a radiation efficiency of 78%. Fabricated on an FR4 substrate with a thickness of 0.8 mm, the antenna ensures a low-profile structure compatible with low-cost, high-volume manufacturing. High isolation between MIMO elements ($S_{12} < -16$ dB) further supports stable multi-port performance. To accelerate the design process, machine learning algorithms
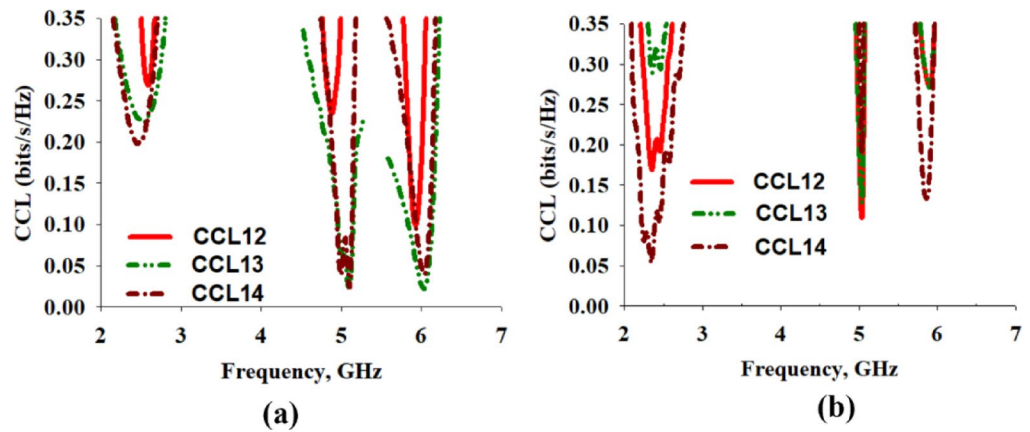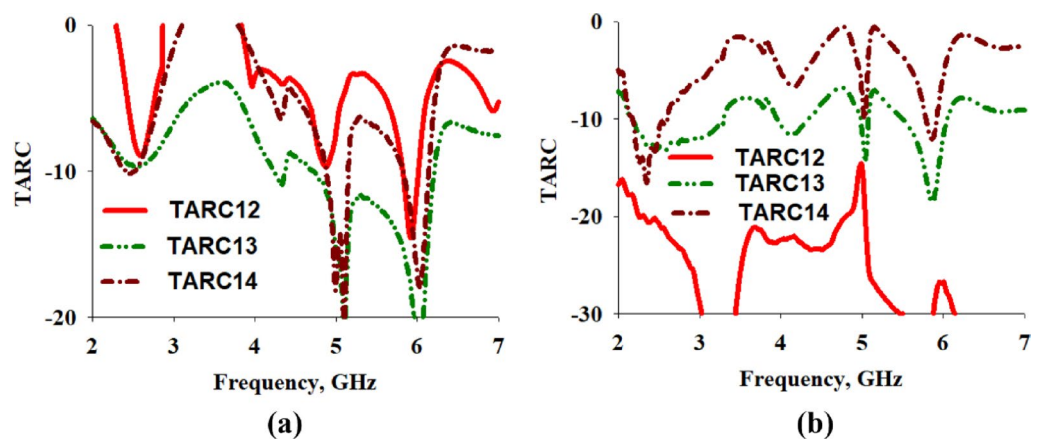
Fig. 12. (**a**) Simulated and (**b**) measured CCL.

Fig. 13. (**a**) Simulated and (**b**) measured TARC.

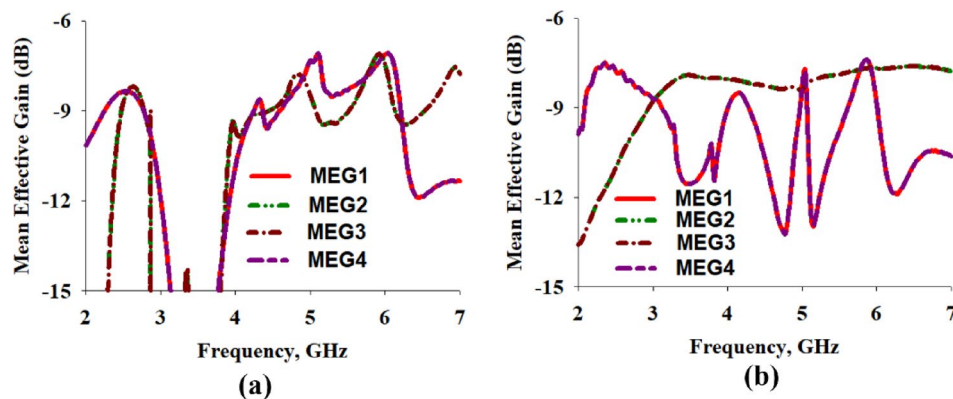**Fig. 14**. (**a**) Simulated and (**b**) measured MEG.

were employed to explore a range of geometric parameters and optimize key metrics such as S_{11}, S_{12}, ECC and DG. For future work, the antenna's real-world integration can be further explored by considering practical constraints such as device packaging, thermal effects, and coexistence with other RF systems. Additionally, scalability analysis is needed to evaluate performance consistency across multiple fabricated units. Another promising direction is the use of lightweight, edge-based ML models for real-time or adaptive reconfiguration of antenna parameters such as beam steering, frequency tuning, or impedance matching based on environmental dynamics.

Data availability
The datasets used and analysed during the current study available from the corresponding author on reasonable request.

References
1. Chen, S.-C., Zhu, J.-L. & Hsu, C.-I.G. Compact double shorted loop sub-6-GHz dual-band MIMO quad-antenna system. *IEEE Access* **9**, 114672–114679. https://doi.org/10.1109/ACCESS.2021.3104306 (2021).
2. Wei, Y. Analysis of spatial diversity technology based on MIMO antenna structures. *Front. Comput. Intell. Syst.* **6**(2), 55–59 (2023).
3. Chen, S.-C., Chiang, C.-W. & Hsu, C.-I.G. Compact four-element MIMO antenna system for 5G laptops. *IEEE Access* **7**, 186056–186064 (2019).
4. Sakli, H., Abdelhamid, C., Essid, C. & Sakli, N. Metamaterial-based antenna performance enhancement for MIMO system applications. *IEEE Access* **9**, 38546–38556 (2021).
5. Sharma, P., Tiwari, R. N., Singh, P. & Kumar, P. MIMO antennas: Design approaches, techniques and applications. *Sensors (Basel)* **22**(20), 7813 (2022).
6. Oughton, E. J. et al. Revisiting wireless internet connectivity: 5G vs Wi-Fi 6. *Telecommun. Policy* **45**(5), 102127 (2021).
7. Xiao, Y. et al. Multiband and low-specific-absorption-rate wearable antenna with low profile based on highly conductive graphene assembled film. *IEEE Antennas Wirel. Propag. Lett.* **22**(9), 2195–2199 (2023).
8. Liu, P. et al. Dual-polarized dipole antenna with dual-band spatial filtering response for aperture-shared triband base station array application. *IEEE Antennas Wirel. Propag. Lett.* **22**(12), 3057–3061 (2023).
9. Huang, N. W., Ji, L.-Y. & Zhou, S.-G. Multiband modified Yagi antenna in a shared transverse aperture. *IEEE Antennas Wirel. Propag. Lett.* **23**(9), 2583–2587 (2024).
10. Liu, S.-B., Zhang, F.-S., Boyuan, M., Gao, S.-P. & Guo, Y.-X. Multiband dual-polarized hybrid antenna with complementary beam for simultaneous RF energy harvesting and WPT. *IEEE Trans. Antennas Propag.* **70**(9), 8485–8495 (2022).
11. Li, Y. J., Ye, L. H., Li, J.-F., Wu, D.-L. & Zhang, X. Y. Triband dual-polarized dipole antenna with controllable bandwidths for 5G/LTE applications. *IEEE Antennas Wirel. Propag. Lett.* **23**(2), 563–567 (2024).
12. Padmanathan, S. et al. Compact multiband reconfigurable MIMO antenna for Sub-6GHz 5G mobile terminal. *IEEE Access* **10**, 60241–60252 (2022).
13. Chung, M.-A., Huang, S.-J., Hsu, C.-C. & Lin, C.-W. A compact and multi-coupled MIMO antenna system applicable to various electronic devices for sub6 GHz design. *IEEE Access* **13**, 60387–60402 (2025).
14. Juan, P.-H. & Su, S.-W. EMC hybrid loop/monopole LDS antenna with three-sided ground walls for 2.4/5/6 GHz WLAN operation. *IEEE Antennas Wirel. Propag. Lett.* **22**(9), 2200–2204 (2023).
15. Chung, M.-A., Hsu, C.-C., Lee, M.-C. & Lin, C.-W. Enhancing multi-band MIMO antenna stability for various electronic applications with human-body interaction consideration. *IEEE Access* **11**, 129376–129398 (2023).
16. Chung, M.-A., Lee, M.-C., Hsu, C.-C. & Lin, C.-W. Multi-band coupled-fed antenna for 4G LTE, sub-6G, and WLAN frequency bands in various electronic devices. *IEEE Access* **12**, 45398–45422 (2024).
17. Chung, M.-A., Hsieh, M.-C., Hsu, C.-C. & Lin, C.-W. A compact multi-band MIMO antenna with high isolation and low SAR for LTE and sub-6 GHz applications. *IEEE Access* **13**, 46014–46029 (2025).
18. Goudos, S. K. et al. Design of antennas through artificial intelligence: State of the art and challenges. *IEEE Commun. Mag.* **60**(12), 96–102 (2022).
19. Wu, Q., Chen, W., Yu, C., Wang, H. & Hong, W. Multilayer machine learning-assisted optimization-based robust design and its applications to antennas and array. *IEEE Trans. Antennas Propag.* **69**(9), 6052–6057 (2021).
20. Wu, Q., Chen, W., Yu, C., Wang, H. & Hong, W. Machine-learning-assisted optimization for antenna geometry design. *IEEE Trans. Antennas Propag.* **72**(3), 2083–2095 (2024).
21. Naous, T. et al. Machine learning-aided design of dielectric-filled slotted waveguide antennas with specified sidelobe levels. *IEEE Access* **10**, 30583–30595 (2022).
22. Syrytsin, I., Pedersen, G. F. & Zhang, S. User effects on mobile phone antennas: Review and potential future solutions. *IEEE Open J. Antennas Propag.* **5**(1), 5–17 (2024).
23. Sharma, Y., Zhang, H. H. & Xin, H. Machine learning techniques for optimizing design of double T-shaped monopole antenna. *IEEE Trans. Antennas Propag.* **68**(7), 5658–5663 (2020).
24. Rai, J. K. et al. Machine learning driven design and optimization of a compact dual Port CPW fed UWB MIMO antenna for wireless communication. *Sci. Rep.* **15**, 13885 (2025).
25. Pusuluri, V. B., Prasad, A. M. & Darimireddy, N. K. Optimization of 5G sub band antenna design using machine learning techniques for WiFi and WiMAX application. *Indian J. Sci. Technol.* **18**(2), 160–167 (2025).
26. Chhaule, N., Koley, C., Mandal, S., Onen, A. & Ustun, T. S. A comprehensive review on conventional and machine learning-assisted design of 5G microstrip patch antenna. *Electronics* **13**, 3819 (2024).
27. Aishwarya, N., Kaur, K. & Seemakurthy, K. A computationally efficient speech emotion recognition system employing machine learning classifiers and ensemble learning. *Int. J. Speech Technol.* **27**, 239–254 (2024).
28. Liu, C. et al. Research progress of computer vision technology in abnormal fish detection. *Aquac. Eng.* **103**, 102350 (2023).
29. Potti, D. et al. A novel optically transparent UWB antenna for automotive MIMO communications. *IEEE Trans. Antennas Propag.* **69**(7), 3821–3828 (2021).
30. Srinubabu, M. & Rajasekhar, N. V. A compact and efficiently designed two-port MIMO antenna for 5G applications. *Heliyon* **10**(7), e28981 (2024).

Acknowledgements

Author contributions
P Devisowjanya proposed the idea, prepared the manuscript regarding the antennas, worked on the simulations and plotted the fabrication results. N Aishwarya prepared the manuscript of machine learning sections and worked on the ML algorithms. Bhanu Sai Mani Kiran Sai called the datasets from CST for ML algorithms. Lokesh Kumar K M worked on the coding of ML algorithms. Arun AAdhithyan S J worked on the fabrication of antenna and analyzing the graphs.

Declarations

Competing interests
The authors declare no competing interests.

Additional information
Correspondence and requests for materials should be addressed to D.P.

Reprints and permissions information is available at www.nature.com/reprints.

Publisher's note Springer Nature remains neutral with regard to jurisdictional claims in published maps and institutional affiliations.